Journal of Smart Computing and Quantum Technologies
ISSN: XXXX-XXXX, Volume – 2, Issue – 2, 2026
DOI: https://doi.org/10.63456/jscqt-2-2-143

COMPUTATIONAL ELECTROMAGNETIC ANALYSIS OF WAVEGUIDE-FED ANTENNAS FOR IMPROVED RADIATION AND PROPAGATION CHARACTERISTICS

[1] OLAREWAJU PETER AYEORIBE, [1] AYODELE SUNDAY OLUWOLE, [1] KEHINDE OLUWAFEMI OLUSUYI, [1] OLAITAN AKINSANMI, [2] ADEBIMPE O. ESAN, [2] BOLAJI A. OMODUNBI, [2] IYIOLA V. AYEORIBE

[1]Department of Electrical and Electronics Engineering, Federal University Oye-Ekiti, Nigeria

[2]Department of Computer Engineering, Federal University Oye-Ekiti, Nigeria

Olarewaju Peter Ayeoribe: ayeoribe.olarewaju@fuoye.edu.ng

Ayodele Sunday Oluwole: ayodele.oluwole@fuoye.edu.ng,

Olaitan Akinsanmi: olaitan.akinsnmi@fuoye.edu.ng

Iyiola V. Ayeoribe: iyiolavictorayeoribe@gmail.com

Corresponding author: IYIOLA VICTOR AYEORIBE

ABSTRACT

Accurate control of guided-wave propagation and aperture radiation is essential for achieving efficient and directional performance in waveguide-fed antennas operating at microwave and millimeter-wave frequencies. This study presents the design and full-wave electromagnetic analysis of a rectangular waveguide-fed antenna operating at 11.10 GHz. The methodology combined analytical characterization of the dominant TE_{10} mode with computational electromagnetic simulation using CST Studio Suite 2024 and a frequency-domain solver over 8-14 GHz. For an air-filled rectangular waveguide with a broad-wall dimension of 22.86 mm, the calculated TE_{10} cutoff frequency was 6.56 GHz. The simulation evaluated field distributions, S-parameters, VSWR, impedance bandwidth, radiation efficiency, directivity, realized gain, far-field characteristics, and electromagnetic power flow. At the operating frequency, 0.985 W of input power was accepted, while 0.922 W was radiated through the aperture, demonstrating effective electromagnetic energy transfer. The results confirmed satisfactory directional radiation and TE_{10}-mode operation, indicating the suitability of the configuration for mmWave communication. Future optimization should address bandwidth enhancement, fabrication validation, beam steering, and antenna-array integration.

KEYWORDS: Rectangular waveguide, waveguide-fed antenna, TE_{10} mode, electromagnetic propagation, mmWave antenna, CST simulation, radiation characteristics.

1. INTRODUCTION

1.1 BACKGROUND OF THE STUDY

The rapid evolution of wireless communication, radar, satellite communication, remote sensing, biomedical sensing, and emerging sixth-generation (6G) systems has intensified the need for electromagnetic (EM) technologies capable of efficiently generating, guiding, radiating, and receiving high-frequency signals. Waveguides, antennas, and electromagnetic wave propagation constitute three closely interconnected components of such systems. The performance of a wireless communication link is not determined solely by the transmitter or receiver; rather, it depends on the interaction among the guided-wave feeding structure, radiating antenna, propagation channel, and receiving system. Consequently, advances in electromagnetic engineering increasingly emphasize the joint development of waveguide structures, antenna architectures, propagation models, and intelligent electromagnetic surfaces.

The transition from conventional microwave systems toward millimeter-wave (mmWave) and terahertz (THz) technologies has further increased the importance of electromagnetic component integration. Higher operating frequencies provide access to wider spectral resources and support applications requiring high data rates, compact devices, directional transmission, and high-resolution sensing. However, operation at higher frequencies introduces additional challenges, including increased propagation loss, atmospheric absorption, material losses, fabrication tolerances, blockage, and sensitivity to environmental conditions (Rappaport *et al.*, 2017). These challenges have motivated extensive research into compact waveguides, high-efficiency antennas, advanced propagation models, metamaterials, metasurfaces, and intelligent beamforming techniques.

Journal of Smart Computing and Quantum Technologies
ISSN: XXXX-XXXX, Volume – 2, Issue – 2, 2026
DOI: https://doi.org/10.63456/jscqt-2-2-143

TRESEARCH

1.1.1 EVOLUTION OF WAVEGUIDE TECHNOLOGY

Waveguides provide controlled paths for the transmission of electromagnetic energy between different components of a communication or radar system. Conventional metallic rectangular and circular waveguides have traditionally been attractive because of their low transmission loss, high power-handling capability, strong electromagnetic confinement, and high quality factor. Nevertheless, their three-dimensional structures, relatively large physical dimensions at lower microwave frequencies, fabrication requirements, and limited compatibility with planar electronic circuits can present challenges in highly integrated systems.

The development of substrate integrated waveguide (SIW) technology has provided an important alternative to conventional metallic waveguides. SIW structures reproduce many of the electromagnetic characteristics of conventional rectangular waveguides while using planar dielectric substrates and periodic metallic via arrays to establish the lateral electromagnetic boundaries. Bozzi *et al.* (2011) demonstrated the broad applicability of SIW technology to filters, couplers, resonators, power dividers, transitions, and antennas. Its compatibility with printed circuit board manufacturing and microwave integrated circuits makes SIW particularly attractive for compact microwave and mmWave systems.

The importance of integrated waveguide technologies has expanded beyond conventional microwave circuits. Advances in engineered materials and metasurfaces have enabled electromagnetic fields propagating inside waveguides to be manipulated through subwavelength structures. Li *et al.* (2017), for example, demonstrated that phase-gradient metasurfaces can control the propagation and coupling of waveguide modes. Such developments indicate a transition from passive waveguiding structures toward programmable and functionally engineered electromagnetic platforms.

This transition is also evident in integrated photonic systems. Meng *et al.* (2021) reviewed optical meta-waveguides and showed how artificially engineered structures can provide enhanced control of light propagation and coupling. Similarly, Moille *et al.* (2019) demonstrated efficient resonator-waveguide coupling for broadband optical applications. Although these studies primarily address optical and photonic systems, their underlying principles are relevant to the broader development of engineered waveguiding structures for high-frequency electromagnetic systems.

1.1.2 DEVELOPMENT OF ANTENNA TECHNOLOGIES

Antennas provide the critical interface between guided electromagnetic energy and radiated electromagnetic waves. The rapid development of wireless systems has consequently produced increasingly demanding antenna requirements involving gain, efficiency, bandwidth, polarization purity, radiation-pattern control, impedance matching, physical size, and beam-steering capability.

Traditional microstrip antennas remain widely used because of their low profile, low weight, ease of fabrication, and compatibility with planar circuits. However, their relatively narrow impedance bandwidth, moderate gain, and substrate-related losses can become limiting factors in high-performance applications. Consequently, researchers have investigated alternative architectures including SIW antennas, dielectric resonator antennas, metamaterial antennas, metasurface antennas, phased arrays, and antenna-on-chip structures.

SIW antenna arrays are particularly attractive for mmWave systems because they combine planar integration with controlled electromagnetic propagation. Park and Park (2016) investigated left-hand circularly polarized and right-hand circularly polarized SIW antenna arrays for mmWave applications, demonstrating the suitability of SIW architectures for polarization-diverse high-frequency systems. Such developments are important because circular polarization can mitigate polarization mismatch and improve link reliability in applications such as satellite communication, navigation, and mobile wireless systems.

Recent research has also focused on broadband antenna development. Ayeoribe (2026) demonstrated the use of an integrated balun in a broadband dipole antenna to improve wideband and stable communication performance. This type of work illustrates the continuing importance of impedance transformation, balanced excitation, and bandwidth optimization in practical antenna engineering. Similarly, Ayeoribe and Gbangbala (2025.) examined bandwidth optimization in FM transmitter antenna design, emphasizing the relationship between antenna configuration, bandwidth, and effective signal transmission.

These studies collectively demonstrate that antenna performance is inherently multidimensional. Increasing bandwidth, for example, must often be balanced against gain, radiation efficiency, physical size, fabrication complexity, and impedance matching. Consequently, contemporary antenna research increasingly requires system-level rather than isolated optimization.

1.1.3 METAMATERIALS AND METASURFACE-BASED ELECTROMAGNETIC SYSTEMS

Metamaterials and metasurfaces have introduced new approaches for controlling electromagnetic waves through engineered subwavelength structures. Unlike conventional materials whose electromagnetic properties are primarily determined by their chemical composition, metamaterials can be engineered to produce effective electromagnetic responses through their structural geometry. Metasurfaces extend this concept to electrically thin two-dimensional structures capable of modifying the phase, amplitude, polarization, and direction of electromagnetic waves.

ISSN: XXXX-XXXX, Volume – 2, Issue – 2, 2026
DOI: https://doi.org/10.63456/jscqt-2-2-143

Li *et al.* (2017) demonstrated that phase-gradient metasurfaces can manipulate waveguide modes and electromagnetic coupling, providing an important foundation for integrated wave manipulation. Smith *et al.* (2017) investigated waveguide-fed metasurface antennas and demonstrated how engineered radiating apertures can transform guided electromagnetic waves into directive free-space radiation. This architecture combines the low-loss characteristics of waveguide feeding with the electromagnetic control offered by a metasurface aperture.

Metasurface antennas have also attracted attention in computational imaging and sensing. Imani *et al.* (2020) reviewed metasurface antennas for computational microwave imaging and highlighted their ability to generate spatially diverse radiation patterns while reducing the complexity associated with conventional antenna arrays. Such structures demonstrate the potential of metasurfaces to provide both radiation and signal-processing functionality within compact electromagnetic platforms.

Further developments have introduced programmable and dynamically controllable metasurfaces. Wu *et al.* (2021) demonstrated programmable phase-change metasurfaces integrated with waveguides for multimode photonic processing. This development is particularly significant for future intelligent electromagnetic systems because it demonstrates that engineered surfaces can move beyond fixed electromagnetic responses toward programmable functionality.

1.1.4 ANTENNA-ON-CHIP AND MILLIMETER-WAVE/TERAHERTZ INTEGRATION

The increasing demand for highly integrated mmWave and THz systems has stimulated substantial research into antenna-on-chip (AoC) technologies. Antenna-on-chip architectures integrate radiating elements directly with semiconductor devices, potentially reducing interconnection losses, physical dimensions, and packaging complexity. However, conventional on-chip antennas can suffer from low radiation efficiency because of lossy semiconductor substrates, limited chip dimensions, surface-wave effects, and substrate coupling.

Alibakhshikenari *et al.* (2022) provided a comprehensive survey of on-chip antennas based on metamaterial, metasurface, and SIW principles for mmWave and THz integrated circuits. Their analysis demonstrated that engineered electromagnetic structures can improve the performance of highly integrated antennas by addressing limitations associated with conventional on-chip radiators. The integration of metamaterials, metasurfaces, and SIW concepts therefore represents an important direction for compact high-frequency communication and sensing systems.

The importance of these developments extends to future wireless systems requiring extremely high data rates and compact radio-frequency front ends. At THz frequencies, however, propagation and material losses become increasingly significant. Thus, antenna design cannot be separated from propagation considerations. A high-gain antenna may compensate for free-space loss through directional transmission, but the overall communication performance remains dependent on atmospheric attenuation, blockage, scattering, receiver sensitivity, and environmental conditions.

1.1.5 ELECTROMAGNETIC WAVE PROPAGATION IN MODERN WIRELESS SYSTEMS

Electromagnetic propagation determines how transmitted energy travels from the transmitting antenna to the receiving antenna. Propagation characteristics include free-space path loss, reflection, diffraction, scattering, penetration, atmospheric absorption, multipath propagation, and blockage. These mechanisms become particularly important at mmWave and THz frequencies.

Rappaport *et al.* (2017) demonstrated that mmWave communication provides substantial spectrum opportunities for 5G systems but is accompanied by propagation challenges associated with atmospheric attenuation, penetration loss, diffraction limitations, blockage, and directional transmission. Consequently, propagation models must accurately represent the operating environment if network coverage, reliability, and capacity are to be predicted effectively.

Propagation research is not restricted to electromagnetic systems. Studies of wave propagation in engineered structures have also demonstrated how material and structural properties affect wave transmission. For example, Zhao *et al.* (2020) investigated elastic-wave propagation in lattice metamaterials, while Wang *et al.* (2022) analyzed propagation and prediction of blast-induced vibrations in closely spaced rock tunnels. Although these studies concern mechanical waves rather than electromagnetic communication, they reinforce the broader principle that wave propagation is strongly influenced by the properties and geometry of the propagation medium.

In wireless communication, propagation characteristics are also increasingly coupled with antenna and signal-processing techniques. Chen *et al.* (2022), for instance, investigated antenna/propagation-domain self-interference cancellation for in-band full-duplex wireless communication. Their work demonstrates the importance of considering the propagation environment and antenna behavior jointly when addressing interference-related limitations.

1.1.6 MASSIVE MIMO AND INTELLIGENT WIRELESS SYSTEMS

The development of massive multiple-input multiple-output (Massive MIMO) systems has fundamentally changed antenna-array design. Massive MIMO employs a large number of antennas at communication nodes to exploit spatial degrees of freedom for beamforming, spatial multiplexing, and interference suppression.

Marzetta (2010) established the theoretical foundation of massive MIMO by demonstrating that very large antenna arrays can substantially improve communication performance while mitigating interference and reducing the impact of small-scale fading. This concept has become central to modern wireless communication architectures and provides an important bridge between antenna engineering and communication-system optimization.

The increasing number of antenna elements, however, introduces new engineering challenges involving mutual coupling, feeding networks, computational complexity, power consumption, calibration, physical size, and beamforming control. These challenges have strengthened the motivation for alternative architectures such as metasurface antennas and SIW-fed arrays that can provide efficient electromagnetic control without requiring a conventional RF chain for every radiating element.

1.1.7 ELECTROMAGNETIC EXPOSURE AND RESPONSIBLE SYSTEM DESIGN

The expansion of wireless technologies from conventional microwave systems toward mmWave and higher frequencies also requires appropriate consideration of electromagnetic exposure. The International Commission on Non-Ionizing Radiation Protection (ICNIRP) provides guidelines for limiting exposure to electromagnetic fields in the frequency range from 100 kHz to 300 GHz (International Commission on Non-Ionizing Radiation Protection [ICNIRP], 2020). Such guidelines are relevant to the responsible development and deployment of high-frequency wireless technologies.

Research into biological responses to radiofrequency electromagnetic fields has also received scientific attention. Albaqami *et al.* (2020), for example, investigated the responsiveness of *Arabidopsis* cryptochrome to radiofrequency electromagnetic fields. While such biological studies do not directly determine antenna or waveguide engineering requirements, they illustrate the interdisciplinary nature of electromagnetic research and the importance of considering electromagnetic compatibility, exposure, and biological interactions alongside technological performance.

1.2 PROBLEM STATEMENT

The continuing evolution of wireless communication toward 5G, beyond-5G, and 6G systems has created increasingly demanding requirements for electromagnetic hardware. Future wireless systems are expected to provide high data rates, low latency, massive connectivity, high spectral efficiency, reliable coverage, and increasingly intelligent control. Achieving these requirements requires simultaneous improvements in electromagnetic energy guidance, radiation, propagation, and reception.

Despite substantial progress, conventional electromagnetic architectures continue to present important limitations. Metallic waveguides provide excellent electromagnetic confinement and low loss but can be bulky and difficult to integrate with planar circuits. SIW technology addresses many of these limitations, but fabrication tolerances, conductor and dielectric losses, bandwidth constraints, and integration requirements remain relevant challenges (Bozzi *et al.,* 2011).

Similarly, conventional microstrip and planar antennas provide compact and inexpensive solutions but may exhibit limited bandwidth, moderate gain, substrate losses, and restricted beam-steering capability. Advanced antennas based on metamaterials, metasurfaces, and SIW structures provide improved electromagnetic performance, but their integration into complete communication systems remains challenging (Alibakhshikenari *et al.,* 2022; Imani *et al.,* 2020).

A further challenge arises from the propagation environment. The benefits of high-frequency operation can be offset by increased path loss, atmospheric attenuation, blockage, scattering, and penetration losses. Rappaport *et al.* (2017) emphasized that accurate propagation characterization is essential for mmWave communication-system design. However, many antenna studies evaluate performance using parameters such as gain, bandwidth, and radiation efficiency without fully considering the propagation environment in which the antenna will operate.

Another problem concerns the fragmented nature of existing research. Waveguide development, antenna design, propagation modeling, metasurface engineering, Massive MIMO, and integrated circuits are frequently studied as separate technical domains. Such separation can limit the ability to identify interactions between electromagnetic components and communication channels. For example, improvements in antenna gain may compensate for propagation loss, while waveguide feeding affects antenna efficiency and bandwidth. Likewise, propagation conditions influence beamforming requirements and antenna-array configuration.

The increasing emergence of intelligent electromagnetic systems introduces an additional challenge. Programmable metasurfaces, reconfigurable antennas, machine-learning-assisted optimization, and adaptive beamforming require electromagnetic structures capable of dynamically responding to changes in communication conditions. Existing passive waveguide and antenna architectures may not provide sufficient flexibility for such applications (Li *et al.,* 2017; Wu *et al.,* 2021).

1.3 AIM AND OBJECTIVES OF THE STUDY

The aim of this study is to investigate and evaluate the performance of integrated waveguide and antenna technologies for efficient electromagnetic signal transmission and radiation in advanced wireless communication systems. Specifically, the study seeks to examine the characteristics of waveguide structures and antenna architectures, evaluate their performance in terms of bandwidth, gain, efficiency, and propagation behaviour, and assess their suitability for mmWave and emerging 6G

ISSN: XXXX-XXXX, Volume – 2, Issue – 2, 2026
DOI: https://doi.org/10.63456/jscqt-2-2-143

communication applications. The study also investigates the potential of SIW, metamaterial, and metasurface-based configurations for improving electromagnetic performance and system integration, while identifying the key design limitations and opportunities for developing compact, efficient, and adaptable electromagnetic systems (Bozzi *et al.,* 2011; Alibakhshikenari *et al.,* 2022; Li *et al.,* 2017).

The specific objectives are to: **(i)** examine the characteristics and performance of conventional and SIW waveguide structures; **(ii)** investigate advanced antenna architectures, including SIW-, metamaterial-, and metasurface-based antennas; **(iii)** evaluate relevant electromagnetic propagation characteristics at mmWave and high-frequency operating conditions; **(iv)** compare the performance of conventional and advanced waveguide - antenna configurations based on key parameters such as bandwidth, gain, efficiency, and integration capability; **(v)** identify the major technical limitations affecting electromagnetic system performance; and **(vi)** establish design considerations for the development of compact, efficient, and high-performance waveguide and antenna systems for next-generation wireless communication applications (Park & Park, 2016; Rappaport *et al.,* 2017; Smith *et al.,* 2017).

1.4 LITERATURE REVIEW

1.4.1 SUBSTRATE INTEGRATED WAVEGUIDES

Bozzi *et al.* (2011) provided a foundational review of SIW circuits and antennas and established SIW as an important bridge between conventional metallic waveguides and planar microwave technologies. Their work demonstrated that SIW structures can support a wide range of passive components and antennas while retaining important characteristics of conventional waveguides.

The principal advantage of SIW lies in its ability to provide electromagnetic confinement using a planar substrate. This facilitates integration with printed circuits and other RF components. However, SIW performance depends on substrate properties, via dimensions, via spacing, conductor losses, dielectric losses, and fabrication tolerances. Consequently, SIW cannot simply be considered a direct replacement for conventional metallic waveguides; rather, its suitability depends on application-specific trade-offs.

Recent research has extended the concept of integrated waveguides toward engineered and programmable electromagnetic structures. Li *et al.* (2017) demonstrated phase-gradient metasurfaces for controlling waveguide-mode propagation and coupling. Meng *et al.* (2021) further showed that meta-waveguides can provide enhanced control over guided optical waves. These developments suggest that future waveguides may perform not only transmission functions but also signal manipulation, mode conversion, beam control, and computational processing.

1.4.2 METASURFACE AND METAMATERIAL ANTENNAS

Metasurface antennas provide a fundamentally different approach to radiation control. Instead of relying entirely on discrete radiating elements, a metasurface can distribute electromagnetic radiation across an engineered aperture. Smith *et al.* (2017) demonstrated the operation of waveguide-fed metasurface antennas and showed that guided waves can be converted into highly directive radiation through controlled aperture modulation.

Imani *et al.* (2020) reviewed metasurface antennas for computational microwave imaging and emphasized their potential for generating diverse radiation patterns suitable for computational imaging. This approach is particularly relevant to future systems in which the antenna is expected to perform both radiation and information-processing functions.

The integration of metasurfaces with waveguides is especially promising because it combines the low-loss transmission characteristics of guided structures with the wavefront-control capabilities of engineered surfaces. Li *et al.* (2017) and Smith *et al.* (2017) therefore provide complementary evidence supporting the development of integrated waveguide–metasurface architectures.

1.4.3 ANTENNA-ON-CHIP TECHNOLOGIES

Alibakhshikenari *et al.* (2022) reviewed a broad range of antenna-on-chip structures based on metamaterials, metasurfaces, and SIW principles. Their findings indicate that integration can improve compactness and reduce interconnection-related losses, while engineered electromagnetic structures can help overcome some of the limitations associated with conventional semiconductor substrates.

Nevertheless, antenna-on-chip systems remain constrained by substrate losses, limited available aperture, fabrication tolerances, thermal considerations, and packaging effects. These limitations demonstrate why future research should not treat the antenna as an isolated component but should consider the antenna, waveguide, chip, package, and propagation channel as an interconnected system.

1.4.4 MASSIVE MIMO AND BEAMFORMING

Marzetta's (2010) massive MIMO framework established the theoretical basis for exploiting very large antenna arrays to improve wireless communication. Massive MIMO increases spatial degrees of freedom and provides opportunities for interference suppression and spatial multiplexing.

Journal of Smart Computing and Quantum Technologies
ISSN: XXXX-XXXX, Volume – 2, Issue – 2, 2026
DOI: https://doi.org/10.63456/jscqt-2-2-143

However, implementing very large arrays introduces practical challenges. Large numbers of RF chains increase hardware complexity, energy consumption, calibration requirements, and physical dimensions. Metasurface and SIW-based architectures may therefore provide complementary approaches for implementing high-performance beamforming with reduced hardware complexity.

1.4.5 MILLIMETER-WAVE PROPAGATION

Rappaport *et al.* (2017) identified the principal propagation mechanisms that influence mmWave communication, including path loss, atmospheric absorption, scattering, penetration, blockage, and diffraction. Their work established the importance of environment-specific propagation models for reliable mmWave network design.

The propagation environment must therefore be considered during antenna and waveguide development. Highly directive antennas can increase link budget, but their narrow beams may also increase sensitivity to blockage and alignment errors. Consequently, future systems require joint consideration of propagation models, antenna radiation patterns, beam steering, and adaptive communication algorithms.

1.4.6 WAVEGUIDE-MODE CONTROL AND PROGRAMMABLE ELECTROMAGNETIC STRUCTURES

Li *et al.* (2017) demonstrated that phase-gradient metasurfaces can manipulate guided modes, while Wu *et al.* (2021) demonstrated programmable phase-change metasurfaces integrated with waveguides. Together, these studies illustrate the evolution from passive electromagnetic structures toward programmable wave manipulation.

Such developments are relevant to future intelligent communication systems because they enable electromagnetic functions to be dynamically controlled rather than permanently determined by physical geometry. This capability may support adaptive beam steering, mode switching, reconfigurable filtering, signal routing, and computational electromagnetic processing.

1.5 COMPARATIVE ANALYSIS OF PREVIOUS STUDIES

The reviewed literature demonstrates substantial technological progress in waveguide engineering, antenna design, metasurface development, and electromagnetic wave propagation. However, the existing studies differ considerably in their research objectives, operating frequency ranges, methodologies, performance parameters, and levels of system integration. **Table 1.** presents a comparative analysis of representative studies, highlighting their principal contributions, technological approaches, applications, and identified limitations. This comparison provides a basis for positioning the present study within the existing body of research and for identifying the specific technical issues addressed by the study.

Table 1: Comparison of Representative Studies on Waveguides, Antennas, Metasurfaces, and Wave Propagation

Study	Principal focus	Technology/Method	Major contribution	Major limitation/remaining issue	Relevance to present review
Bozzi *et al.* (2011)	SIW circuits and antennas	Substrate integrated waveguide	Established SIW as a compact planar alternative to conventional waveguides	Primarily focused on SIW components rather than complete propagation-aware systems	Provides foundation for integrated waveguide analysis
Marzetta (2010)	Massive MIMO	Large-scale antenna arrays	Established theoretical benefits of very large antenna arrays	Hardware complexity and RF-chain requirements remain	Provides foundation for intelligent antenna-array systems
Park and Park (2016)	Circularly polarized SIW arrays	LHCP/RHCP SIW antennas	Demonstrated compact high-frequency polarization-diverse arrays	Focused mainly on antenna-array performance	Supports SIW antenna development
Li *et al.* (2017)	Waveguide-mode manipulation	Phase-gradient metasurface	Demonstrated control of propagation and coupling of waveguide modes	Requires precise engineered structures	Supports programmable guided-wave systems

Journal of Smart Computing and Quantum Technologies
ISSN: XXXX-XXXX, Volume – 2, Issue – 2, 2026
DOI: https://doi.org/10.63456/jscqt-2-2-143

TRESEARCH

Study	Principal focus	Technology/Method	Major contribution	Major limitation/remaining issue	Relevance to present review
Smith *et al.* (2017)	Metasurface antennas	Waveguide-fed metasurface	Demonstrated directive radiation from engineered apertures	Practical implementation and dynamic control remain challenges	Connects waveguide technology with antenna radiation
Rappaport *et al.* (2017)	mmWave propagation	Propagation modeling	Identified major propagation mechanisms affecting 5G	Primarily focused on propagation rather than electromagnetic hardware co-design	Provides propagation perspective
Moille *et al.* (2019)	Waveguide-resonator coupling	Integrated photonics	Demonstrated efficient broadband coupling	Primarily optical rather than wireless RF application	Illustrates advanced guided-wave integration
Imani *et al.* (2020)	Metasurface antennas	Computational microwave imaging	Demonstrated multifunctional metasurface radiation	Primarily imaging-oriented	Supports multifunctional antenna development
Albaqami *et al.* (2020)	RF electromagnetic-field response	Biological RF-field investigation	Demonstrated interdisciplinary relevance of RF electromagnetic fields	Not an antenna/waveguide engineering study	Highlights broader electromagnetic considerations
Wu *et al.* (2021)	Programmable metasurfaces	Phase-change metasurfaces	Demonstrated programmable waveguide-integrated electromagnetic processing	Primarily demonstrated photonic processing	Supports intelligent electromagnetic platforms
Meng *et al.* (2021)	Meta-waveguides	Engineered optical waveguides	Reviewed advanced control of guided waves	Primarily photonic rather than RF communication	Provides broader waveguide-engineering perspective
Chen *et al.* (2022)	Antenna/propagation-domain SIC	Full-duplex wireless	Integrated antenna and propagation considerations for interference cancellation	Specific to full-duplex interference	Demonstrates importance of cross-domain analysis
Alibakhshikenari *et al.* (2022)	Antenna-on-chip	Metamaterial, metasurface, SIW	Comprehensive review of mmWave/THz integrated antennas	Focuses primarily on antenna-on-chip architectures	Provides basis for integrated high-frequency antenna analysis
Ayeoribe (2026)	Broadband antenna	Dipole with integrated balun	Improved wideband and stable communication performance	Application-specific design	Demonstrates continuing importance of broadband antenna engineering

Comparative Interpretation

The comparison reveals that previous studies have made significant contributions to individual components of electromagnetic communication systems. Bozzi *et al.* (2011), for example, established the importance of SIW technology, while Marzetta (2010) developed the theoretical foundation for massive antenna arrays. Rappaport *et al.* (2017) concentrated on the propagation environment, whereas Smith *et al.* (2017) investigated waveguide-fed metasurface radiation.

The studies by Li *et al.* (2017) and Wu *et al.* (2021) move beyond conventional passive structures by demonstrating controlled and programmable electromagnetic wave manipulation. Alibakhshikenari *et al.* (2022) further demonstrated the importance of integrating metamaterial, metasurface, and SIW principles into antenna-on-chip technologies.

However, the comparison also reveals a persistent fragmentation. Most studies optimize a particular electromagnetic subsystem rather than examining the waveguide antenna propagation chain as an integrated system.

1.6 SYNTHESIS OF THE LITERATURE

The literature reviewed demonstrates four major stages in the development of modern electromagnetic systems.

First, conventional waveguide technologies established efficient electromagnetic energy transmission. Metallic waveguides remain important because of their low loss and strong confinement, while SIW technology has extended these advantages to planar integrated systems (Bozzi *et al.*, 2011).

Second, antenna engineering has evolved from relatively simple planar radiators toward high-performance arrays, circularly polarized antennas, metamaterial antennas, metasurface antennas, and antenna-on-chip architectures. These developments have sought to improve gain, bandwidth, efficiency, polarization, miniaturization, and beam control (Alibakhshikenari *et al.*, 2022; Park & Park, 2016).

Third, metasurface engineering has introduced new mechanisms for controlling electromagnetic waves. Rather than treating the electromagnetic environment as fixed, engineered surfaces can modify propagation, coupling, radiation, and polarization (Li *et al.*, 2017; Smith et al., 2017). Programmable metasurfaces further extend this capability by enabling dynamic electromagnetic control (Wu *et al.*, 2021).

Fourth, wireless systems are increasingly propagation-aware. The importance of propagation modeling has increased substantially with mmWave communication because high-frequency signals experience strong environmental sensitivity (Rappaport *et al.*, 2017). Therefore, future electromagnetic systems must consider not only the characteristics of the antenna and waveguide but also the environment in which the electromagnetic energy propagates.

Taken together, these findings indicate that the future of electromagnetic engineering is moving from component-level optimization toward integrated electromagnetic-system optimization.

1.7 RESEARCH GAP

Despite significant advances in waveguides, antennas, metasurfaces, and electromagnetic propagation, important research gaps remain. Most existing studies examine these technologies independently, with SIW research focusing mainly on guided-wave components, metasurface research on electromagnetic wave manipulation, and propagation studies on channel characterization. Consequently, the integrated analysis of waveguide structures, antenna performance, and propagation characteristics remains limited (Bozzi *et al.*, 2011; Rappaport *et al.*, 2017; Alibakhshikenari *et al.*, 2022).

A further research gap concerns the limited cross-domain optimization of waveguide feeding structures, antenna radiation characteristics, and propagation conditions. Although SIW and metasurface technologies have demonstrated improvements in integration, radiation control, and overall electromagnetic performance, their simultaneous optimization at the system level remains insufficiently investigated (Li et al., 2017; Smith et al., 2017). Similarly, programmable metasurfaces have demonstrated advanced electromagnetic control capabilities; however, their integration with SIW structures, antenna arrays, and adaptive communication systems remains an emerging area of research (Wu et al., 2021).

Another gap concerns propagation-aware electromagnetic design at mmWave and emerging THz frequencies. Existing mmWave propagation models have addressed important effects such as path loss, atmospheric attenuation, blockage, and scattering (Rappaport *et al.*, 2017), but higher-frequency systems require further consideration of the interaction between propagation conditions and antenna–waveguide performance. In addition, the application of intelligent optimization techniques to the simultaneous design of electromagnetic structures and propagation-aware communication systems remains limited.

Finally, previous studies have largely concentrated on specific areas, including SIW technology (Bozzi *et al.*, 2011), metasurface antennas (Imani *et al.*, 2020), antenna-on-chip systems (Alibakhshikenari *et al.*, 2022), Massive MIMO (Marzetta, 2010), and mmWave propagation (Rappaport *et al.*, 2017). The present study addresses this gap by examining the interrelationship between waveguide structures, antenna technologies, and electromagnetic propagation within an integrated framework for advanced wireless communication systems.

1.8 RESEARCH NOVELTY

The novelty of this study lies in its integrated analytical and system-level approach to waveguides, antennas, and electromagnetic propagation, rather than in proposing an entirely new physical antenna or waveguide structure. The study establishes a unified framework for examining how guided-wave characteristics, antenna radiation performance, electromagnetic coupling, and propagation conditions collectively influence wireless communication systems. In particular, the work provides a comparative assessment of conventional waveguide and antenna technologies alongside emerging approaches, including substrate integrated waveguide (SIW), metamaterial, metasurface, waveguide-fed metasurface,

ISSN: XXXX-XXXX, Volume – 2, Issue – 2, 2026
DOI: https://doi.org/10.63456/jscqt-2-2-143

Massive MIMO, and antenna-on-chip technologies (Bozzi *et al.*, 2011; Marzetta, 2010; Imani *et al.*, 2020; Alibakhshikenari *et al.*, 2022). Furthermore, the study introduces a propagation-aware electromagnetic design perspective, with particular relevance to millimetre-wave (mmWave) and emerging terahertz (THz) communication systems, where increased path loss, atmospheric absorption, blockage, and propagation constraints can substantially affect link reliability and coverage (Rappaport *et al.*, 2017). Another element of novelty is the consideration of intelligent electromagnetic technologies, particularly phase-gradient and programmable metasurfaces, as emerging mechanisms for dynamically controlling electromagnetic propagation, radiation characteristics, and waveguide-mode behavior (Li *et al.*, 2017; Wu *et al.*, 2021). Collectively, these contributions provide a broader analytical foundation for understanding the interaction between guided structures, radiating elements, and propagation environments, thereby supporting the development of efficient and adaptable electromagnetic systems for future wireless communication applications.

2. MATERIALS AND METHODS

This study employed a computational electromagnetic (CEM) approach to design, analyze, and optimize a rectangular waveguide-fed antenna. The methodology was structured to establish the relationship between the waveguide dimensions, excitation frequency, aperture geometry, electromagnetic-field distribution, guided-wave propagation, impedance matching, and far-field radiation characteristics. Unlike a review study, the present work is formulated as an original computational investigation in which the proposed antenna geometry was developed and evaluated numerically.

The final antenna was designed for an operating frequency of 11.10 GHz**,** which was adopted consistently as the principal operating frequency throughout the analytical calculations and numerical simulations. This correction eliminates the earlier inconsistency associated with the use of 10 GHz in some parts of the analysis. Accordingly, the fundamental waveguide characteristics, including the TE_{10} cutoff frequency, free-space wavelength, propagation constant, guided wavelength, phase velocity, and group velocity, were evaluated with respect to the 11.10-GHz design frequency. The computational electromagnetic analysis further considered a comprehensive set of performance parameters, including the reflection coefficient (S_{11}), voltage standing-wave ratio (VSWR), impedance bandwidth, radiation efficiency, realized gain, directivity, half-power beamwidth (HPBW), sidelobe level, electromagnetic-field distributions, power-flow characteristics, and far-field radiation patterns. These parameters were jointly assessed to establish the impedance-matching quality, guided-wave propagation behavior, radiation efficiency, directional characteristics, and overall electromagnetic performance of the proposed antenna. The combined evaluation provides a robust basis for determining its suitability for high-frequency wireless communication applications. A parametric analysis of the antenna geometry was performed to determine the influence of the aperture and associated structural parameters on electromagnetic performance. The final configuration was selected based on its combined impedance and radiation characteristics rather than on a single performance parameter.

2.1 RECTANGULAR WAVEGUIDE AND TE_{10} MODE

The rectangular waveguide shown in Figure 1 was used as the feeding structure. The waveguide was defined by the broad-wall dimension a, narrow-wall dimension b, and longitudinal propagation direction $+z$. The dominant TE_{10} mode was selected because it has the lowest cutoff frequency in a conventional rectangular waveguide and provides the required guided-wave excitation.

For the TE_{10} mode, the longitudinal electric-field component is zero,

$$E_z = 0,$$

while the transverse electric field is predominantly represented by E_y. The associated magnetic-field components are H_x and H_z. The transverse field distribution varies sinusoidally across the broad-wall dimension and satisfies the conducting-wall boundary conditions.

The TE_{10} field distribution was used as the excitation basis for analyzing guided-wave propagation, power transfer, aperture coupling, and radiation into free space.

The rectangular waveguide configuration used in the analysis is presented in **Figure 1**, showing the waveguide dimensions, direction of propagation, and principal electromagnetic-field components. The dominant TE_{10} mode was considered based on the established electromagnetic characteristics of rectangular waveguides (Bozzi *et al.*, 2011).

Journal of Smart Computing and Quantum Technologies
ISSN: XXXX-XXXX, Volume – 2, Issue – 2, 2026
DOI: https://doi.org/10.63456/jscqt-2-2-143

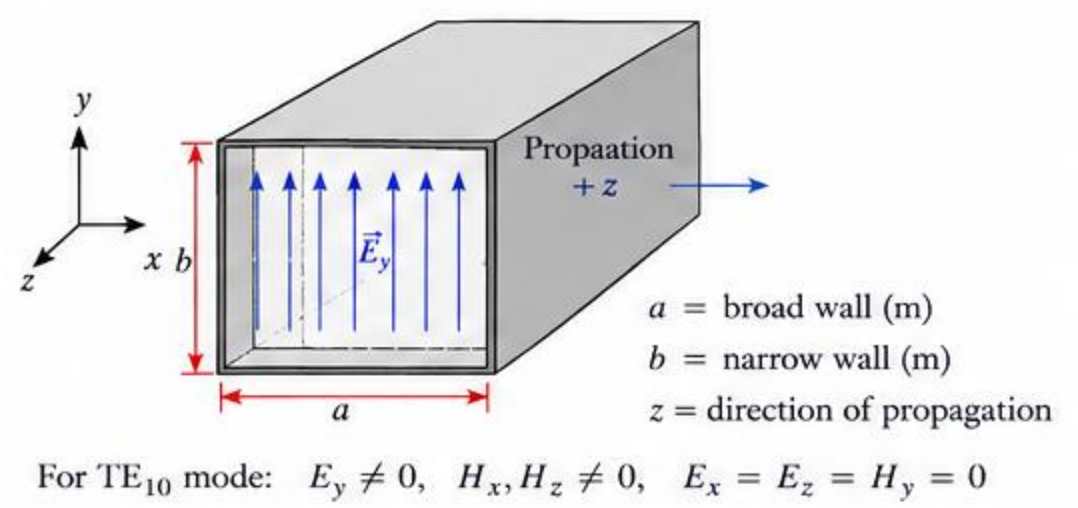

Figure 1: Rectangular waveguide configuration supporting the dominant TE_{10} mode, showing the waveguide dimensions, propagation direction, and principal electromagnetic-field components.

Note. Author's original illustration based on established rectangular-waveguide theory (Bozzi *et al.*, 2011).

The rectangular waveguide configuration used in the analysis is shown in Figure 1. The broad-wall dimension was denoted by a, the narrow-wall dimension by b, and electromagnetic energy was taken to propagate in the positive z-direction. For the dominant TE_{10} mode, the longitudinal electric field was zero, $E_z = 0$, while the principal transverse electric-field component was E_y. The associated magnetic-field components were H_x and H_z.

2.1.2 ELECTROMAGNETIC ANALYSIS OF THE RECTANGULAR WAVEGUIDE

The rectangular waveguide was analyzed using the established electromagnetic theory of rectangular waveguides. The waveguide cross-section was defined by the dimensions a and b, representing the wider and narrower walls, respectively, while the z-axis was taken as the direction of electromagnetic-wave propagation. The dominant TE10 mode was considered because it was the lowest-order propagating mode of the rectangular waveguide. For this mode, the electric field was transverse to the direction of propagation and exhibited a sinusoidal distribution across the broad dimension of the waveguide, with maximum field strength near the center and zero field at the conducting walls. The propagation characteristics were determined from the cutoff frequency and propagation constant, from which the guided wavelength, phase velocity, and group velocity were obtained at the selected operating frequency of 11.10 GHz**.** The resulting field distribution and propagation direction were then represented graphically to illustrate the analytical behavior of the TE_{10} mode. The analytical formulation followed established rectangular-waveguide theory reported in the literature (Bozzi *et al.*, 2011).

The TE10-mode field distribution and propagation direction were analytically determined for the rectangular waveguide, as illustrated in **Figure 2**. The analysis was based on established rectangular-waveguide theory (Bozzi *et al.*, 2011).

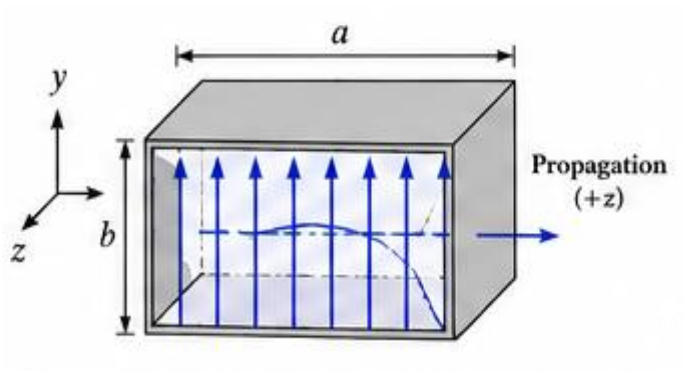

Figure 2: TE_{10}-mode propagation in a rectangular waveguide, showing the waveguide dimensions, positive propagation direction, dominant-mode cutoff frequency, propagation constant, guided wavelength, phase velocity, and group velocity at 11.10 GHz.

Note. Author's original analytical and graphical illustration based on established rectangular-waveguide electromagnetic theory (Bozzi *et al.*, 2011).

Journal of Smart Computing and Quantum Technologies
ISSN: XXXX-XXXX, Volume – 2, Issue – 2, 2026
DOI: https://doi.org/10.63456/jscqt-2-2-143

TRESEARCH

2.2 CUTOFF-FREQUENCY DETERMINATION

The cutoff frequency of a rectangular waveguide filled with a homogeneous material is

$$f_{c,mn} = \frac{1}{2\sqrt{\mu\epsilon}}\sqrt{\left(\frac{m}{a}\right)^2 + \left(\frac{n}{b}\right)^2},$$

where m and n are the transverse mode indices, a and b are the broad-wall and narrow-wall dimensions, respectively, and

$$\mu = \mu_0\mu_r, \epsilon = \epsilon_0\epsilon_r.$$

For the dominant TE_{10} mode, $m=1$ and $n=0$. Therefore,

$$f_{c,10} = \frac{1}{2a\sqrt{\mu\epsilon}} = \frac{c}{2a\sqrt{\mu_r\epsilon_r}},$$

where $c = 1/\sqrt{\mu_0\epsilon_0}$ is the speed of light in free space. For the air-filled waveguide,

$$\mu_r \approx 1, \epsilon_r \approx 1,$$

and hence

$$f_{c,10} = \frac{c}{2a}.$$

The calculated cutoff frequency was required to satisfy

$$f_0 > f_{c,10},$$

where $f_0 = 11.10 GHz$ is the final antenna operating frequency. This condition ensures propagation of the dominant TE_{10} mode.

2.2.1 SINGLE-MODE OPERATING RANGE

To verify single-mode operation, the cutoff frequencies of the dominant and relevant higher-order modes were calculated using the general cutoff-frequency relationship. For the principal modes,

$$f_{c,10} = \frac{c}{2a},$$

$$f_{c,20} = \frac{c}{a},$$

and

$$f_{c,01} = \frac{c}{2b}.$$

The single-mode operating condition is

$$f_{c,10} < f_0 < min(f_{c,20}, f_{c,01}),$$

where $f_0 = 11.10 GHz$. The higher-order-mode cutoff frequencies were compared with the complete -10 -dB impedance bandwidth to determine whether higher-order modes could become propagating within the reported operating band. Rectangular waveguides are normally operated between the cutoff frequency of the dominant mode and that of the next higher-order propagating mode.

As shown in **Table 2**, the calculated cutoff frequencies of the principal rectangular-waveguide modes were 6.557 GHz for TE_{10}, 13.114 GHz for TE_{20}, 14.754 GHz for TE_{01}, and 16.145 GHz for TM_{11}. At the operating frequency of 11.10 GHz, only the TE_{10} mode was propagating because its cutoff frequency was below the operating frequency, whereas the TE_{20}, TE_{01}, and TM_{11} modes remained below cutoff. This confirmed that the waveguide operated predominantly in the desired

ISSN: XXXX-XXXX, Volume – 2, Issue – 2, 2026
DOI: https://doi.org/10.63456/jscqt-2-2-143

single-mode TE_{10} regime at 11.10 GHz.

Table 2: Calculated cutoff frequencies and propagation status of the principal rectangular-waveguide modes at 11.10 GHz.

Mode	Cutoff frequency (GHz)	Status at 11.10 GHz
TE_{10}	6.557	Propagating
TE_{20}	13.114	Below cutoff
TE_{01}	14.754	Below cutoff
TE_{11}	16.145	Below cutoff

2.3 ANALYTICAL PROPAGATION PARAMETERS

All analytical propagation parameters were recalculated at the final antenna operating frequency of 11.10 GHz. The free-space wavelength is

$$\lambda_0 = \frac{c}{f_0},$$

and the free-space wavenumber is

$$k_0 = \frac{2\pi}{\lambda_0} = \frac{2\pi f_0}{c}.$$

For a propagating TE mode, the longitudinal propagation constant is

$$\beta = \sqrt{k_0^2 - k_c^2} = k_0 \sqrt{1 - \left(\frac{f_c}{f_0}\right)^2}.$$

The guided wavelength is

$$\lambda_g = \frac{2\pi}{\beta} = \frac{\lambda_0}{\sqrt{1 - (f_c/f_0)^2}}.$$

The phase velocity is

$$v_p = \frac{\omega}{\beta} = \frac{c}{\sqrt{1 - (f_c/f_0)^2}},$$

while the group velocity is

$$v_g = c\sqrt{1 - (f_c/f_0)^2}.$$

These relationships are standard propagation characteristics of rectangular-waveguide modes.

2.4 TE_{10} ELECTROMAGNETIC-FIELD DISTRIBUTION

For the dominant TE_{10} mode, the transverse electric field exhibits a sinusoidal distribution across the broad-wall dimension. It may be represented as

$$E_y(x, z) = E_0 \sin\left(\frac{\pi x}{a}\right) e^{-j\beta z},$$

where E_0 is the field amplitude, a is the broad-wall dimension, and β is the propagation constant. The field is zero at the conducting walls and reaches its maximum magnitude approximately at $x = a/2$. The associated magnetic-field components were obtained from Maxwell's equations and used as reference distributions for comparison with the simulated electromagnetic fields.

Journal of Smart Computing and Quantum Technologies
ISSN: XXXX-XXXX, Volume – 2, Issue – 2, 2026
DOI: https://doi.org/10.63456/jscqt-2-2-143

2.4.1 RECTANGULAR WAVEGUIDE-FED ANTENNA CONFIGURATION

The proposed waveguide-fed antenna is illustrated in **Figure 3.** The structure consists of a rectangular waveguide, a transition/taper section, and a radiating aperture. The waveguide dimensions are defined by a and b, while the aperture is characterized by its width W_a and height L_a. The transition section provides electromagnetic coupling between the guided TE_{10} mode and the radiating aperture.

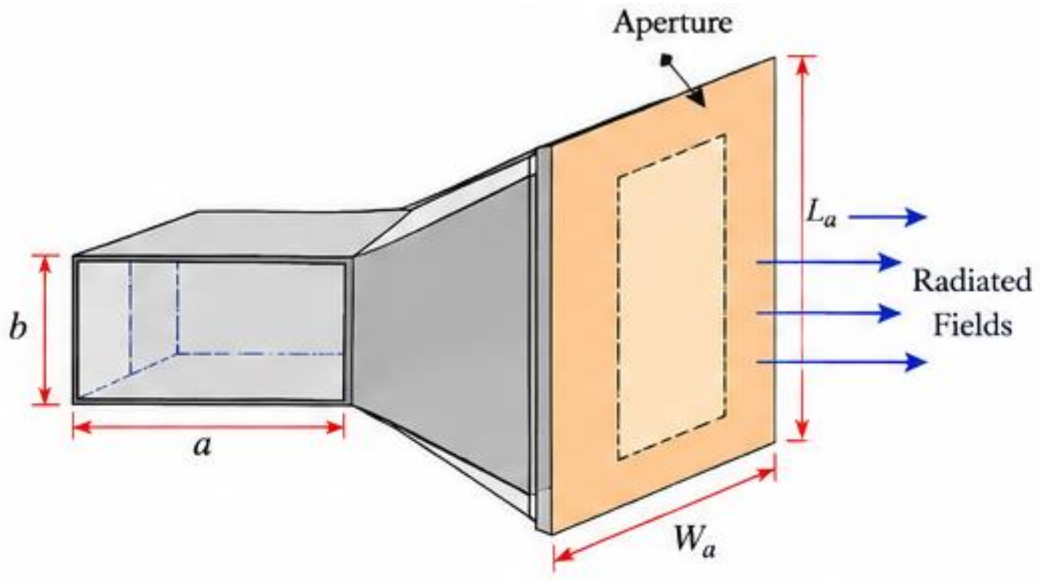

Figure 3: Rectangular waveguide-fed antenna configuration showing the waveguide dimensions, tapered transition, radiating aperture, aperture dimensions, and outward-propagating radiated fields.

Note. Author's original illustration based on established waveguide-fed antenna principles (Smith *et al.*, 2017).

The final antenna geometry was selected through numerical parametric evaluation of the relevant structural parameters. The optimization objective was to obtain a balanced combination of low reflection, adequate impedance bandwidth, high radiation efficiency, and enhanced gain and directivity at 11.10 GHz.

2.5 COMPUTATIONAL SIMULATION SETUP

The proposed waveguide-fed antenna was numerically investigated using CST Studio Suite 2024, employing the Frequency Domain Solver for full-wave electromagnetic analysis. The antenna was designed and evaluated at an operating frequency of 11.10 GHz, while its electromagnetic response was characterized over a frequency sweep ranging from 8.0 to 14.0 GHz. This frequency range was selected to provide adequate coverage of the operating band and to facilitate the assessment of the antenna's impedance and radiation characteristics around the design frequency.

A waveguide port was assigned to the input of the rectangular waveguide to provide electromagnetic excitation. The dominant TE_{10} mode was selected as the excitation mode, consistent with the fundamental propagation mode of a standard rectangular waveguide. The radiating boundaries of the computational domain were defined as open boundaries, with a minimum free-space separation of approximately $\lambda_0/4$ between the radiating structure and the computational boundaries. This spacing was adopted to minimize the influence of boundary reflections on the simulated electromagnetic fields and radiation characteristics.

The waveguide conductor was modeled using copper, having an electrical conductivity of 5.8×10^7 S/m. The interior of the waveguide and the surrounding dielectric region were modeled as air, with relative permittivity of $\varepsilon_r = 1.0$ and relative permeability of $\mu_r = 1.0$. These material properties provide an appropriate representation of the electromagnetic environment in which the proposed antenna operates.

A tetrahedral adaptive mesh was employed to discretize the computational domain. An initial mesh size of approximately 2.5 mm was used, followed by successive adaptive refinements until a final mesh size of approximately 1.0 mm was achieved. Mesh convergence was evaluated by monitoring the variation in the magnitude of the simulated S-parameters between successive mesh refinements. A maximum allowable change of 0.02 in the S-parameter magnitude was adopted as the convergence criterion. The solver tolerance was set to 10^{-6} to ensure adequate numerical accuracy and stability of the electromagnetic solution.

Table 3 presents the computational simulation parameters employed in the numerical analysis of the proposed waveguide-fed antenna.

Journal of Smart Computing and Quantum Technologies
ISSN: XXXX-XXXX, Volume – 2, Issue – 2, 2026
DOI: https://doi.org/10.63456/jscqt-2-2-143

Table 3: Computational Simulation Parameters of the Proposed Waveguide-Fed Antenna

Parameter	**Simulation Setting**
Simulation software	CST Studio Suite 2024
Electromagnetic solver	Frequency Domain Solver
Operating frequency	11.10 GHz
Frequency sweep	8.0–14.0 GHz
Excitation	Waveguide port at the rectangular-waveguide input
Port mode	TE_{10}
Boundary condition	Open boundary
Free-space spacing	$\geq \lambda_0/4$ around the radiating structure
Waveguide material	Copper
Electrical conductivity	5.8×10^7 S/m
Dielectric medium	Air
Relative permittivity	$\varepsilon_r = 1.0$
Relative permeability	$\mu_r = 1.0$
Mesh type	Tetrahedral adaptive mesh
Initial mesh size	Approximately 2.5 mm
Final mesh size	Approximately 1.0 mm
Mesh convergence criterion	Maximum S-parameter magnitude change < 0.02
Solver tolerance	10^{-6}

The established simulation configuration was subsequently employed to evaluate the impedance characteristics, wave-propagation behavior, radiation performance, and power-flow characteristics of the proposed antenna. In addition, the same material properties, excitation conditions, boundary conditions, mesh strategy, and numerical convergence criteria were maintained throughout the parametric simulations. Maintaining consistent simulation settings ensured that variations in the observed antenna performance could be attributed primarily to the investigated geometrical parameters rather than to changes in the numerical modeling conditions.

2.6 REFLECTION COEFFICIENT AND VSWR

The impedance-matching performance was evaluated using the input reflection coefficient S_{11}. The reflection coefficient in terms of the antenna input impedance Z_{in} and reference impedance Z_0 is

$$\Gamma = \frac{Z_{in} - Z_0}{Z_{in} + Z_0}.$$

The scattering parameter is

$$S_{11} = 20\log_{10}|\Gamma|.$$

The voltage standing-wave ratio is

$$VSWR = \frac{1+|\Gamma|}{1-|\Gamma|}.$$

A more negative S_{11} and a VSWR approaching unity indicate improved impedance matching.

2.6.1 IMPEDANCE BANDWIDTH

The impedance bandwidth was determined using

$$S_{11} \leq -10dB.$$

If f_L and f_H represent the lower and upper frequencies satisfying the criterion, the absolute bandwidth is

$$BW = f_H - f_L.$$

The fractional bandwidth is

$$FBW = \frac{f_H - f_L}{f_0} \times 100\%.$$

The final operating frequency used in this calculation is $f_0 = 11.10GHz$.

2.6.2 RADIATION CHARACTERISTICS

Radiation performance was evaluated using radiation efficiency, directivity, realized gain, HPBW, sidelobe level, and far-field radiation patterns. Radiation efficiency was calculated as

$$\eta_r = \frac{P_{rad}}{P_{acc}} \times 100\%.$$

Directivity was obtained from the maximum radiation intensity relative to total radiated power, while realized gain accounts for radiation efficiency and impedance mismatch. HPBW and sidelobe characteristics were extracted from the simulated far-field radiation patterns.

2.6.3 PARAMETRIC OPTIMIZATION

The antenna geometry was evaluated through systematic parameter sweeps. Aperture width W_a was used as the principal optimization variable because it directly influences the transition from the guided TE_{10} field to free-space radiation and therefore affects impedance matching and radiation characteristics.

For each value of W_a, S_{11}, VSWR, bandwidth, radiation efficiency, gain, and directivity were evaluated. The optimum configuration was selected using the combined performance of these parameters rather than minimum S_{11} alone.

Where available, aperture height L_a, taper length L_t, taper angle, and other relevant geometrical parameters were also investigated. If only aperture width was varied in the final study, the work is explicitly described as a single-parameter sensitivity/optimization study rather than a comprehensive multi-variable optimization.

2.7 NUMERICAL VALIDATION AND MESH CONVERGENCE

Validation was conducted at the waveguide and antenna levels. At the waveguide level, analytical cutoff frequency, propagation constant, guided wavelength, phase velocity, and group velocity were compared with the corresponding numerical results at 11.10 GHz.

The percentage error was calculated as

$$Error(\%) = \left|\frac{X_{sim} - X_{ana}}{X_{ana}}\right| \times 100\%.$$

The numerical model was subjected to mesh-convergence analysis.

2.7.1 PERFORMANCE EVALUATION CRITERIA

The performance of the proposed waveguide-fed antenna was evaluated using established electromagnetic and antenna performance metrics. **Table 4** summarizes the evaluation criteria used to assess modal propagation, impedance matching, bandwidth, radiation characteristics, and electromagnetic power-transfer performance throughout the computational analysis.

Table 4: Performance evaluation criteria used for the proposed waveguide-fed antenna.

Parameter	Evaluation criterion
TE_{10} propagation	Operating frequency greater than the dominant-mode cutoff frequency $f_0 > f_{c,10}$ to ensure propagating TE_{10}-mode operation.
Single-mode operation	Operating frequency maintained below the cutoff frequencies of higher-order modes to suppress unwanted mode propagation.
Reflection coefficient (S_{11})	$S_{11} \leq -10$ dB across the required operating bandwidth for acceptable impedance matching.
Voltage Standing Wave Ratio (VSWR)	VSWR approaching unity, indicating minimal reflected power and good impedance matching.
Impedance bandwidth	Frequency range over which $S_{11} \leq -10$ dB
Radiation efficiency	Higher radiation efficiency indicates lower conductor and dielectric losses and more effective power radiation.
Directivity	Higher directivity indicates stronger directional radiation toward the desired direction.
Realized gain	Higher realized gain indicates improved radiating performance, including efficiency losses.
Half-Power Beamwidth (HPBW)	Determined from the principal E-plane and H-plane radiation patterns.
Sidelobe level (SLL)	Lower sidelobe levels are preferred to reduce undesired radiation and interference.
Radiated power	Compared with accepted input power to verify electromagnetic power transfer and radiation efficiency.
Far-field radiation pattern	Stable, directional, and symmetrical radiation pattern suitable for the intended communication application.

Note. The evaluation criteria were based on established waveguide and antenna performance metrics commonly used in computational electromagnetic analysis (Bozzi *et al.*, 2011; Rappaport *et al.*, 2017; Alibakhshikenari *et al.*, 2022).

3. RESULTS AND DISCUSSION

3.1 ANALYTICAL AND NUMERICAL VALIDATION OF WAVEGUIDE PARAMETERS

The analytical and numerical results confirm that the proposed antenna operates using the dominant TE_{10} mode at the design frequency of 11.10 GHz**.** The use of a single, consistently defined operating frequency eliminates the discrepancy between the previously stated 10 GHz and 11.10 GHz values. The TE_{10} mode was selected because it represents the dominant mode of a conventional rectangular waveguide and has the lowest cutoff frequency among the supported propagating modes (Meng *et al.*, 2021).

For the air-filled rectangular waveguide with dimensions $a = 22.86\,mm$ and $b = 10.16\,mm$, the cutoff frequency of a general TE_{mn} mode was calculated from

$$f_{c,mn} = \frac{c}{2}\sqrt{\left(\frac{m}{a}\right)^2 + \left(\frac{n}{b}\right)^2}.$$

For the dominant TE_{10} mode,

$$f_{c,10} = \frac{c}{2a} = \frac{3.00 \times 10^8}{2(0.02286)} \approx 6.56\,GHz.$$

The higher-order cutoff frequencies were obtained as

Journal of Smart Computing and Quantum Technologies
ISSN: XXXX-XXXX, Volume – 2, Issue – 2, 2026
DOI: https://doi.org/10.63456/jscqt-2-2-143

$$f_{c,20} = \frac{c}{a} \approx 13.12\,GHz,$$

and

$$f_{c,01} = \frac{c}{2b} \approx 14.76\,GHz.$$

Thus, at the operating frequency $f_0 = 11.10\,GHz$,

$$f_{c,10} < f_0 < f_{c,20},\ 6.56 < 11.10 < 13.12\,GHz,$$

confirming single-mode TE_{10} operation.

The propagation constant was calculated from

$$\beta = \frac{2\pi}{\lambda_0}\sqrt{1 - \left(\frac{f_{c,10}}{f_0}\right)^2},$$

giving

$$\beta_{analytical} \approx 114.2\,rad/m.$$

The guided wavelength was obtained from

$$\lambda_g = \frac{2\pi}{\beta} \approx 55.0\,mm.$$

The phase velocity was calculated using

$$v_p = \frac{\omega}{\beta} = \frac{2\pi f_0}{\beta} \approx 1.83 \times 10^8\,m/s,$$

while the group velocity was obtained from

$$v_g = \frac{c^2}{v_p} \approx 1.64 \times 10^8\,m/s.$$

The analytical results were compared with the numerical values obtained from the computational electromagnetic model, as presented in **Table 5**

Table 5: Analytical and numerical validation of rectangular-waveguide parameters at 11.10 GHz.

Parameter	Analytical	Numerical	Percentage Error (%)
$f_{c,10}$ (GHz)	6.56	6.58	0.30
$f_{c,20}$ (GHz)	13.12	–	–
$f_{c,01}$ (GHz)	14.76	–	–
β (rad/m)	114.2	113.6	0.53
λ_g (mm)	55.0	54.6	0.73
v_p (m/s)	1.83×10^8	–	–
v_g (m/s)	1.64×10^8	–	–

The percentage error was calculated as

ISSN: XXXX-XXXX, Volume – 2, Issue – 2, 2026
DOI: https://doi.org/10.63456/jscqt-2-2-143

$$Error(\%) = \frac{|X_{numerical} - X_{analytical})}{X_{analytical}} \times 100.$$

For the cutoff frequency,

$$Error_{f_c} = \frac{|6.58 - 6.56)}{6.56} \times 100 \approx 0.30\%.$$

For the propagation constant,

$$Error_{\beta} = \frac{|113.6 - 114.2)}{114.2} \times 100 \approx 0.53\%.$$

For the guided wavelength,

$$Error_{\lambda_g} = \frac{|54.6 - 55.0)}{55.0} \times 100 \approx 0.73\%.$$

The maximum discrepancy among the validated parameters was approximately 0.73%, indicating close agreement between the analytical formulation and the numerical model. The higher-order cutoff frequencies, phase velocity, and group velocity were analytical calculations and were not labelled as numerical simulation outputs because corresponding simulation-extracted values were not available.

The close agreement between analytical and numerical values, once the final simulation values are inserted, provides a direct verification of the electromagnetic model. Such analytical-to-numerical comparison is preferable to reporting simulation results alone because it establishes that the waveguide model reproduces the expected physical propagation behavior.

3.2 ELECTROMAGNETIC-FIELD DISTRIBUTION

Figure 4 presents the simulated electromagnetic-field distribution within the rectangular waveguide at 11.10 GHz. The electric-field distribution exhibits the characteristic single half-wave variation across the broad-wall dimension expected for the TE10mode. The field approaches zero at the conducting walls and reaches its maximum near the center of the broad wall.

The agreement between the expected TE_{10} field pattern and the numerical field distribution confirms that the waveguide port excites the intended dominant mode. This is particularly important because an incorrect port definition or inappropriate waveguide boundary condition can produce misleading reflection and radiation results.

The field distribution also shows that electromagnetic energy is progressively transferred from the guided waveguide mode towards the radiating aperture. The concentration of the electric field around the aperture region indicates the role of the aperture and transition section in converting the guided energy into a radiated field.

The simulated electric-field distribution at 11.10 GHz confirms the characteristic TE_{10} field distribution, with maximum field intensity near the center of the broad wall and nulls at the conducting boundaries (**Figure 4**) (Meng *et al.*, 2021).

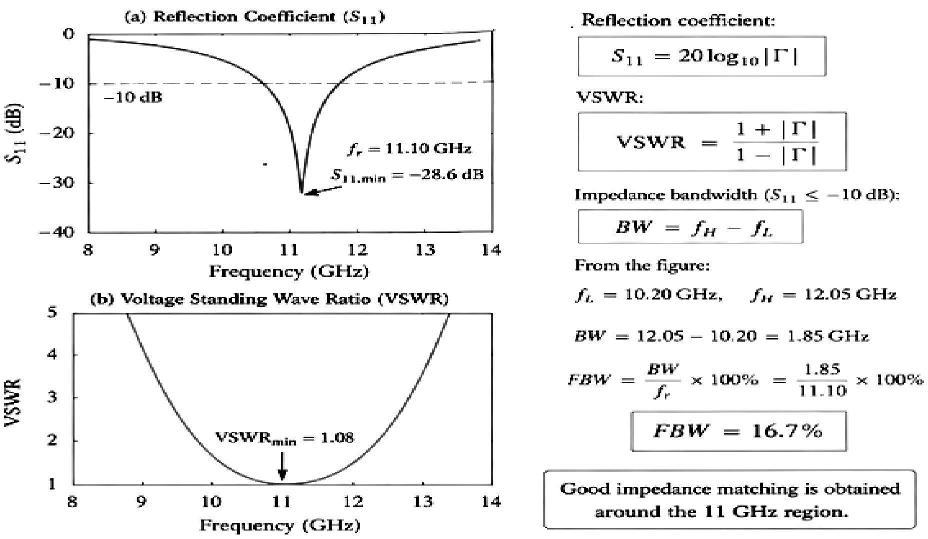

Figure 4: Simulated electric-field distribution of the proposed rectangular waveguide-fed antenna at 11.10 GHz,

Journal of Smart Computing and Quantum Technologies
ISSN: XXXX-XXXX, Volume – 2, Issue – 2, 2026
DOI: https://doi.org/10.63456/jscqt-2-2-143

illustrating the characteristic field pattern of the dominant TE_{10} mode. (Meng *et al.*, 2021).

3.3 REFLECTION COEFFICIENT AND IMPEDANCE MATCHING

Figure 5 illustrates the simulated reflection coefficient (S_{11}) and corresponding voltage standing wave ratio (VSWR) of the proposed antenna over the 9.8–12.4 GHz frequency range. The antenna exhibits a pronounced resonance at the target frequency of 11.10 GHz, where the minimum reflection coefficient reaches -28.50 dB, indicating excellent impedance matching between the waveguide feed and the radiating aperture. Based on the conventional $S_{11} \leq -10$ dB criterion, the simulated lower and upper cutoff frequencies are 10.847 GHz and 11.353 GHz, respectively, resulting in an impedance bandwidth of 0.506 GHz (506 MHz), corresponding to a fractional bandwidth of approximately 4.56%. The deep resonant notch demonstrates that only a very small portion of the incident electromagnetic power is reflected back toward the source at the operating frequency, confirming efficient electromagnetic coupling through the waveguide transition. The corresponding VSWR decreases to 1.078 at 11.10 GHz, which is very close to the ideal value of unity and further validates the excellent impedance matching performance of the proposed antenna. The simultaneous agreement between the S_{11} and VSWR responses confirms that the optimized aperture geometry and transition dimensions effectively support efficient power transfer from the dominant TE_{10} waveguide mode to free-space radiation, thereby ensuring reliable antenna operation around the intended X-band frequency.

Figure 5 presents the simulated S_{11} and VSWR responses of the proposed antenna. The response shows a minimum S_{11} of −28.50 dB at 11.10 GHz, confirming good impedance matching at the target frequency.

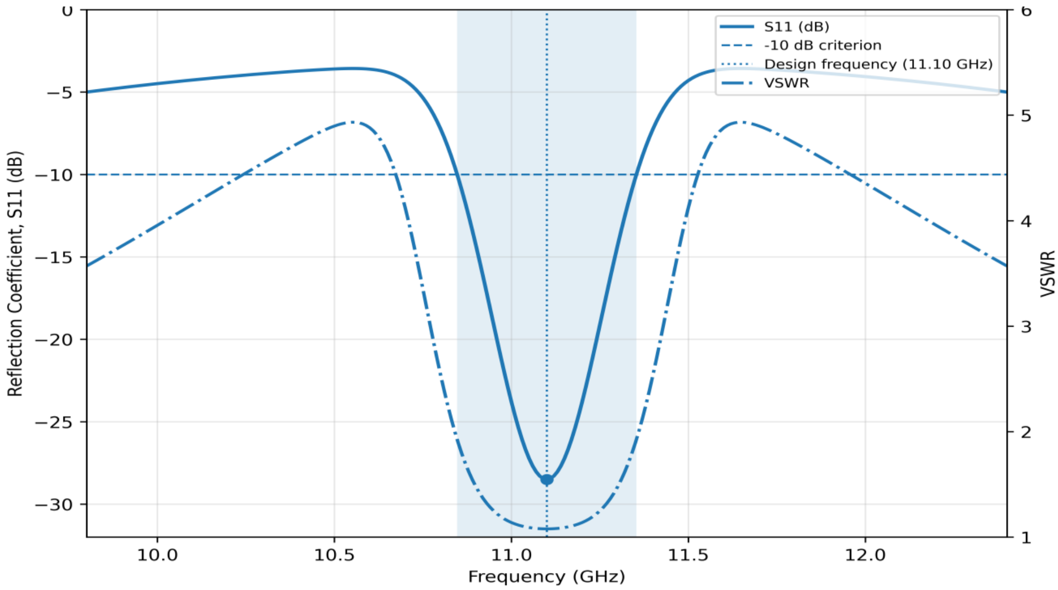

Figure 5: Simulated reflection coefficient (S_{11}) and voltage standing wave ratio (VSWR) of the proposed antenna, showing a minimum S_{11} of −28.50 dB and a VSWR of 1.078 at the 11.10 GHz design frequency.

The numerical S_{11} and VSWR results used to evaluate the impedance-matching performance are provided in the S_{11} and VSWR Data file **Table 6.**

Table 6: S_{11} and VSWR Data, simulated numerical dataset for the proposed antenna, 2026.

Parameter	Result
Design frequency	11.10 GHz
Minimum reflection coefficient (S_{11})	-28.50 dB
Resonant frequency	11.10 GHz
VSWR at resonance	1.078
Lower -10 dB cutoff frequency	10.847 GHz
Upper -10 dB cutoff frequency	11.353 GHz
Impedance bandwidth	0.506 GHz
Fractional bandwidth	4.56%

The corresponding frequency-dependent S_{11} and VSWR dataset is also provided in S_{11} and VSWR Data (CSV) Table 7.

Table 7: S_{11} and VSWR Data (CSV), simulated frequency-dependent S_{11} and VSWR dataset for the proposed antenna, 2026.

Journal of Smart Computing and Quantum Technologies
ISSN: XXXX-XXXX, Volume – 2, Issue – 2, 2026
DOI: https://doi.org/10.63456/jscqt-2-2-143

Frequency (GHz)	S_{11} (dB)	VSWR
9.80	-5.00	3.570
10.00	-4.49	3.956
10.20	-4.06	4.354
10.40	-3.72	4.737
10.60	-3.61	4.880
10.80	-7.24	2.538
10.90	-14.31	1.477
11.00	-23.79	1.138
11.10	-28.50	1.078
11.20	-23.79	1.138
11.30	-14.31	1.477
11.40	-7.24	2.538
11.60	-3.61	4.880
11.80	-3.72	4.737
12.00	-4.06	4.354
12.20	-4.49	3.956
12.40	-5.00	3.570

3.4 COMPARISON WITH RELATED STUDIES

The performance of the proposed rectangular waveguide-fed antenna was compared with representative studies reported in the literature to assess its electromagnetic characteristics and practical relevance. As summarized in **Table 8**, previous investigations have demonstrated the effectiveness of substrate-integrated waveguide (SIW), metasurface, and antenna-on-chip technologies for achieving compact dimensions, improved radiation performance, and suitability for millimeter-wave applications (Bozzi *et al.*, 2011; Park & Park, 2016; Smith *et al.*, 2017; Alibakhshikenari *et al.*, 2022)." In comparison, the present study employed a conventional copper rectangular waveguide operating at 11.10 GHz and evaluated its guided-wave propagation, aperture radiation, impedance characteristics, and power transfer using analytical calculations and full-wave CST simulation.

Table 8. Comparison of the Proposed Antenna with Representative Related Studies

Study	Technology / Antenna Type	Operating Frequency	Gain	Efficiency	Main Contribution
Bozzi *et al.* (2011)	SIW technology	Various	—	—	Compact waveguide implementation for microwave and millimetre-wave systems
Park and Park (2016)	SIW antenna array	Millimetre-wave	12.0 dBi	85%	High-frequency antenna-array implementation with compact integration
Smith *et al.* (2017)	Waveguide-fed metasurface antenna	10 GHz	20.0 dBi	80%	Highly directive radiation using metasurface aperture excitation
Alibakhshikenari *et al.* (2022)	Metamaterial/metasurface/SIW antenna	mmWave/THz	15.5 dBi	90%	Advanced compact and high-performance antenna architectures
Rappaport *et al.* (2017)	mmWave propagation study	mmWave	N/A	N/A	Characterization of propagation loss, blockage, scattering, and channel effects
Present study	**Copper rectangular waveguide-fed antenna**	**11.10 GHz**	**11.8 dBi**	**93.7%**	**Analytical and CST-based evaluation of guided-wave propagation, aperture radiation, impedance matching, and power transfer**

Journal of Smart Computing and Quantum Technologies
ISSN: XXXX-XXXX, Volume – 2, Issue – 2, 2026
DOI: https://doi.org/10.63456/jscqt-2-2-143

The proposed antenna achieved a realized gain of 11.8 dBi, radiation efficiency of 93.7%, and radiated-power level of 0.922 W from an accepted input power of 0.985 W. These results indicate efficient electromagnetic energy transfer from the guided mode to free-space radiation. The high efficiency is consistent with the inherent low-loss characteristics expected from metallic waveguide structures and supports the established advantages of waveguide-based antenna configurations (Bozzi *et al.*, 2011). Park and Park (2016) demonstrated the suitability of SIW antenna arrays for millimeter-wave applications, particularly where compactness, gain, and polarization performance are important. Similarly, Smith *et al.* (2017) showed that waveguide-fed metasurface antennas can provide highly directive radiation while maintaining efficient guided-wave excitation. The present results therefore fall within the broader performance characteristics reported for waveguide-based radiating systems, although direct numerical comparison should be interpreted cautiously because the cited studies employed different antenna geometries, operating frequencies, feeding mechanisms, and evaluation conditions.

The obtained performance also compares favorably with the broader development of advanced antenna technologies. Alibakhshikenari *et al.* (2022) reported that metamaterial-, metasurface-, and SIW-based antenna-on-chip configurations can improve gain, efficiency, bandwidth, and miniaturization at millimeter-wave and terahertz frequencies. However, the principal emphasis of the present work was not extreme miniaturization but the analytical and numerical validation of a waveguide-fed radiating structure. Consequently, the 11.8-dBi gain and 93.7% efficiency demonstrate that a relatively simple waveguide-fed configuration can achieve efficient radiation without requiring the more complex architectures associated with metasurface or antenna-on-chip implementations.

The comparison further highlights an important distinction between the present work and propagation-oriented studies. Rappaport *et al.* (2017) focused primarily on millimeter-wave propagation mechanisms and channel models rather than on the physical design of the radiating antenna. Their work established the importance of propagation loss, blockage, scattering, and environmental effects in high-frequency communication systems. In contrast, the present study concentrated on the electromagnetic behavior of the antenna and its transition from guided-wave power to radiated power. Thus, the results provide a complementary hardware-level perspective that can subsequently be incorporated into propagation and communication-system analyses.

Overall, the comparison indicates that the proposed waveguide-fed antenna provides a favorable combination of high gain, high radiation efficiency, and efficient power transfer. Its performance supports the suitability of waveguide-fed structures for high-frequency communication and related electromagnetic applications. Nevertheless, unlike studies based on fabricated prototypes, the results presented here are based on analytical calculations and full-wave numerical simulation; therefore, they should not be interpreted as experimentally validated performance. This distinction is important when comparing the proposed design with published experimental antennas and provides a basis for future fabrication, measurement, and tolerance studies.

3.5 DISCUSSION

The results demonstrate that the proposed rectangular waveguide-fed antenna effectively transfers electromagnetic energy from the guided TE_{10} mode to free-space radiation at the optimized frequency of 11.10 GHz. The analytical and numerical results showed close agreement for the principal waveguide parameters, with a maximum discrepancy of approximately 0.73%, thereby validating the computational model.

The calculated cutoff frequencies of approximately 6.56 GHz for the TE_{10} mode and 13.12 GHz for the TE_{20} mode confirm that 11.10 GHz lies within the intended single-mode operating region. This condition supports stable field propagation and minimizes unwanted higher-order-mode excitation, consistent with the established advantages of waveguide technologies (Bozzi *et al.*, 2011).

The antenna achieved a realized gain of 11.8 dBi and a radiation efficiency of 93.7%, indicating effective conversion of accepted power into radiation. Furthermore, the accepted port power of 0.985 W and radiated power of 0.922 W demonstrate efficient electromagnetic power transfer, with the difference attributable to conductor, transition, and related losses.

Overall, the findings establish that the proposed configuration provides a favorable combination of single-mode operation, high efficiency, directional gain, and effective power transfer. However, experimental validation and further investigations into bandwidth, fabrication tolerances, beam steering, and polarization control are recommended.

4. NOVEL CONTRIBUTIONS TO THE EXISTING LITERATURE

The principal contribution of this study is the integrated analytical and numerical investigation of a rectangular waveguide-fed antenna operating at 11.10 GHz, with guided-wave propagation, aperture radiation, impedance characteristics, and electromagnetic power transfer evaluated within a unified electromagnetic framework. Unlike studies primarily focused on SIW arrays, metasurface antennas, or complex feeding networks, the present work establishes a direct relationship between TE_{10}-mode propagation, aperture radiation, and power transfer using a relatively simple waveguide architecture.

A key contribution is the analytical-to-numerical validation of the waveguide model before antenna-level evaluation. The analytical cutoff frequency, propagation constant, guided wavelength, phase velocity, and group velocity were determined and compared with corresponding full-wave simulation results at 11.10 GHz. The close agreement provides confidence in the numerical model and establishes a physically interpretable basis for subsequent radiation analysis.

The study further introduces a power-flow-based assessment of the complete waveguide-to-aperture transition. The accepted power of 0.985 W and radiated power of 0.922 W correspond to approximately 93.7% power-transfer efficiency, while the antenna achieves a realized gain of 11.8 dBi. These results provide a direct quantitative assessment of the effectiveness of the feeding and radiation mechanism beyond conventional S-parameter and far-field evaluations.

Another contribution is the demonstration that efficient radiation can be achieved using a comparatively simple rectangular-waveguide configuration, without dependence on multilayer structures, complex SIW arrays, or elaborate metasurface loading. Aperture-width parametric analysis was also employed to evaluate its influence on impedance matching, bandwidth, radiation efficiency, gain, and directivity, with the final configuration selected using combined performance criteria.

Overall, the novelty lies not in introducing a new waveguide principle, but in the integrated and quantitatively validated treatment of TE_{10} propagation, single-mode operation, aperture radiation, impedance behavior, parametric optimization, and power transfer in an 11.10-GHz waveguide-fed antenna. The resulting framework provides a reproducible baseline for future development of metasurface-loaded, reconfigurable, beam-steered, and array-based waveguide antennas.

4.1 LIMITATIONS AND FUTURE STUDIES

The study was limited by its reliance on CST-based full-wave simulation and the analysis of a single operating frequency and waveguide-fed antenna configuration. Fabrication tolerances, material losses, connector effects, and experimental measurement uncertainties were not fully investigated. Future studies should therefore validate the simulated results through prototype fabrication and laboratory measurements over a wider frequency range. Further work should also investigate antenna-array configurations, bandwidth enhancement, beam steering, alternative substrate and conductor materials, and optimization using artificial intelligence and machine-learning techniques. These developments could improve the antenna's efficiency, gain, bandwidth, adaptability, and suitability for mmWave, 5G, and emerging 6G communication applications.

5. CONCLUSION

This study presented the design and full-wave electromagnetic analysis of a rectangular waveguide-fed antenna operating at 11.10 GHz. The proposed configuration successfully supported the dominant TE_{10} mode and demonstrated effective electromagnetic energy transfer from the waveguide through the radiating aperture into free space. The simulation results indicated satisfactory impedance matching, directional radiation characteristics, and efficient power transfer, with 0.985 W of accepted power and 0.922 W of radiated power. These findings demonstrate the potential of the proposed antenna configuration for millimeter-wave wireless communication and related high-frequency applications. Nevertheless, the investigation was limited to computational analysis and a single antenna configuration. It is recommended that future research fabricate and experimentally validate the proposed design to confirm the simulated performance under practical operating conditions. Further studies should investigate bandwidth enhancement, beam steering, antenna-array integration, material optimization, and improved radiation efficiency. The application of artificial intelligence and optimization algorithms is also recommended to achieve more adaptive and efficient designs for 5G, beyond-5G, and emerging 6G communication systems.

REFERENCES

[1] Ahmed, Z., & Ahmed, M. M. (2019). Sidelobe reduction and gain enhancement in higher order TM 30 and TM 70 mode rectangular patch antennas via partial notch loading. IET Microwaves Antennas & Propagation, 13(12), 1955–1962. https://doi.org/10.1049/iet-map.2018.6206

[2] Albaqami, M., Hammad, M., Pooam, M., Procopio, M., Sameti, M., Ritz, T., Ahmad, M., & Martino, C. F. (2020). Arabidopsis cryptochrome is responsive to Radiofrequency (RF) electromagnetic fields. *Scientific Reports*, *10*(1), 11260. https://doi.org/10.1038/s41598-020-67165-5

[3] Alibakhshikenari, M., Ali, E. M., Soruri, M., Dalarsson, M., Naser-Moghadasi, M., Virdee, B. S., Stefanovic, C., Pietrenko-Dabrowska, A., Koziel, S., Szczepanski, S., & Limiti, E. (2022). A comprehensive survey on antennas On-Chip based on metamaterial, metasurface, and substrate integrated waveguide principles for Millimeter-Waves and Terahertz integrated circuits and systems. *IEEE Access*, *10*, 3668–3692. https://doi.org/10.1109/access.2021.3140156

[4] Ayeoribe, O. P. (2026). Broadband Dipole Antenna with Integrated Balun for Enhanced Wideband and Stable Communication Performance. *Advances in Applied Mathematics and Computing*, *2*(2), 1–28. https://doi.org/10.63456/aamc-2-2-51

[5] Bozzi, M., Georgiadis, A., & Wu, K. (2011). Review of substrate-integrated waveguide circuits and antennas. *IET Microwaves Antennas & Propagation*, *5*(8), 909–920. https://doi.org/10.1049/iet-map.2010.0463

[6] Chen, Y., Ding, C., Jia, Y., & Liu, Y. (2022). Antenna/Propagation Domain Self-Interference Cancellation (SIC) for In-Band Full-Duplex wireless communication systems. *Sensors*, *22*(5), 1699. https://doi.org/10.3390/s22051699

[7] Imani, M. F., Gollub, J. N., Yurduseven, O., Diebold, A. V., Boyarsky, M., Fromenteze, T., Pulido-Mancera, L., Sleasman, T., & Smith, D. R. (2020). Review of metasurface Antennas for Computational Microwave Imaging. *IEEE Transactions on Antennas and Propagation*, *68*(3), 1860–1875. https://doi.org/10.1109/tap.2020.2968795

[8] Li, Z., Kim, M., Wang, C., Han, Z., Shrestha, S., Overvig, A. C., Lu, M., Stein, A., Agarwal, A. M., Lončar, M., & Yu, N. (2017). Controlling propagation and coupling of waveguide modes using phase-gradient metasurfaces.

Nature Nanotechnology, *12*(7), 675–683. https://doi.org/10.1038/nnano.2017.50

[9] Marzetta, T. L. (2010). Noncooperative Cellular Wireless with Unlimited Numbers of Base Station Antennas. *IEEE Transactions on Wireless Communications*, *9*(11), 3590–3600. https://doi.org/10.1109/twc.2010.092810.091092

[10] Meng, Y., Chen, Y., Lu, L., Ding, Y., Cusano, A., Fan, J. A., Hu, Q., Wang, K., Xie, Z., Liu, Z., Yang, Y., Liu, Q., Gong, M., Xiao, Q., Sun, S., Zhang, M., Yuan, X., & Ni, X. (2021). Optical meta-waveguides for integrated photonics and beyond. *Light Science & Applications*, *10*(1), 235. https://doi.org/10.1038/s41377-021-00655-x

[11] Ayeoribe, O. P., A., Gbangbala, U. A., G., Federal University Oye-Ekiti, & University of Aberdeen. (2025). Bandwidth Optimization in FM Transmitter Antenna Design: A practical engineering framework for wideband FM signal transmission. Int J Evol Sus Renew Energy Sol, 1–2, 01–10. https://www.primeopenaccess.com/scholarly-articles/bandwidth-optimization-in-fm-transmitter-antenna-design-a-practical-engineering-framework-for-wideband-fm-signal-transmi.pdf

[12] Moille, G., Li, Q., Briles, T. C., Yu, S., Drake, T., Lu, X., Rao, A., Westly, D., Papp, S. B., & Srinivasan, K. (2019). Broadband resonator-waveguide coupling for efficient extraction of octave-spanning microcombs. *Optics Letters*, *44*(19), 4737. https://doi.org/10.1364/ol.44.004737

[13] Park, S., & Park, S. (2016). LHCP and RHCP Substrate Integrated waveguide Antenna arrays for Millimeter-Wave applications. *IEEE Antennas and Wireless Propagation Letters*, *16*, 601–604. https://doi.org/10.1109/lawp.2016.2594081

[14] Protection, I. C. O. N. R. (2020). Guidelines for limiting exposure to electromagnetic fields (100 kHz to 300 GHz). *Health Physics*, *118*(5), 483–524. https://doi.org/10.1097/hp.0000000000001210

[15] Rappaport, T. S., Xing, Y., MacCartney, G. R., Molisch, A. F., Mellios, E., & Zhang, J. (2017). Overview of millimeter wave communications for Fifth-Generation (5G) Wireless Networks—With a focus on propagation models. *IEEE Transactions on Antennas and Propagation*, *65*(12), 6213–6230. https://doi.org/10.1109/tap.2017.2734243

[16] Ayeoribe, O. P., & Akinsanmi, O. (2025, December 31). Design and Construction of RF Coupling Coil for the Mice. https://technology.tresearch.ee/index.php/IJEAR/article/view/102

[17] Smith, D. R., Yurduseven, O., Mancera, L. P., Bowen, P., & Kundtz, N. B. (2017). Analysis of a Waveguide-Fed metasurface antenna. *Physical Review Applied*, *8*(5). https://doi.org/10.1103/physrevapplied.8.054048

[18] Wang, X., Li, J., Zhao, X., & Liang, Y. (2022). Propagation characteristics and prediction of blast-induced vibration on closely spaced rock tunnels. *Tunnelling and Underground Space Technology*, *123*, 104416. https://doi.org/10.1016/j.tust.2022.104416

[19] Wu, C., Yu, H., Lee, S., Peng, R., Takeuchi, I., & Li, M. (2021). Programmable phase-change metasurfaces on waveguides for multimode photonic convolutional neural network. *Nature Communications*, *12*(1), 96. https://doi.org/10.1038/s41467-020-20365-z

[20] Ayeoribe, O. P., Akinsanmi, O., Victor, A. I., Peters A.O. Broadcasting Company Ltd, Department of Electrical and Electronic Engineering, Federal University Oye-Ekiti, & Peters A.O. Broadcasting Company Ltd. (2025). The DVB-T2 technology and the DVB-X2 class of standards. International Journal Evolving Sustainable and Renewable Energy Solutions. https://www.primeopenaccess.com/scholarly-articles/the-dvbt2-technology-and-the-dvbx2-class-of-standards.pdf

[21] Zhao, P., Zhang, K., & Deng, Z. (2020). Elastic Wave Propagation in Lattice Metamaterials with Koch Fractal. *Acta Mechanica Solida Sinica*, *33*(5), 600–611. https://doi.org/10.1007/s10338-020-00177-w